Test of a theoretical equation of state for elemental solids and liquids

Eric D. Chisolm, Scott D. Crockett, and Duane C. Wallace

Theoretical Division, Los Alamos National Laboratory

Los Alamos, NM 87545

February 1, 2008

Abstract

We propose a means for constructing highly accurate equations of state (EOS) for elemental solids and liquids essentially from first principles, based upon a particular decomposition of the underlying condensed matter Hamiltonian for the nuclei and electrons. We also point out that at low pressures the neglect of anharmonic and electron-phonon terms, both contained in this formalism, results in errors of less than 5% in the thermal parts of the thermodynamic functions. Then we explicitly display the forms of the remaining terms in the EOS, commenting on the use of experiment and electronic structure theory to evaluate them. We also construct an EOS for Aluminum and compare the resulting Hugoniot with data up to 5 Mbar, both to illustrate our method and to see whether the approximation of neglecting anharmonicity et al. remains viable to such high pressures. We find a level of agreement with experiment that is consistent with the low-pressure results.

1   Introduction

Over approximately the last sixty years, numerous models and techniques have been developed for creating equations of state (EOS) for a variety of materials that are valid up to very extreme pressures (tens of Mbar) and

temperatures (several eV). In the EOS community at the national laboratories, for instance, we have often used models based on the Mie-Grüneisen EOS together with the Thomas-Fermi or Thomas-Fermi-Dirac model (or one of its modifications) to include the contributions from the electrons (see [1] for examples). The models usually contain enough independent parameters to adjust the EOS until it correctly reproduces the experimentally measured Hugoniot (and perhaps a few other data points), but it is generally an open question how accurate the EOS is away from the Hugoniot. In this paper we argue that for one class of materials, elemental solids and liquids, our understanding of the underlying condensed matter Hamiltonian for the nuclei and electrons has grown to the point that we can construct highly accurate EOS from essentially first principles, and we also propose a means for doing so. We also argue that, since the underlying physics is well understood, an EOS derived this way should have the right functional form, even if we are unsure of the values of some of its parameters; thus, if the resulting EOS is shown to be accurate in one thermodynamic region (say, along the Hugoniot), then we can be confident that it is roughly equally accurate elsewhere.

In this formalism, the EOS in the solid phase depends on a decomposition of the Hamiltonian due to Wallace (see Chapter 1 of [2]), extending the work of Born [3] to metals as well as insulators; the resulting free energy contains terms describing the harmonic motion of the nuclei about their lattice sites (phonons), thermal excitation of the electrons from their ground state, anharmonic corrections to the nuclear motion (represented as phonon-phonon interactions), and interactions between the electron excitations and the nuclear motion, represented as electron-phonon interactions. (Please note that this description is exact; all of the physics contained in the true Hamiltonian of the system is included here. Specific EOS models usually neglect the anharmonic and electron-phonon terms, arguing that anharmonicity is small and making reference to some form of the Born-Oppenheimer approximation; we will take a somewhat different route, commenting on approximations below.) A recently developed theory of the dynamics of monatomic liquids (see [4] for a review) uses the same Hamiltonian to derive a liquid free energy which is quite similar to the expression for a solid, with additional terms accounting for the fact that the liquid, as opposed to the solid, traverses many potential valleys and thus sees the boundaries between them. For both phases, the resulting free energies have been compared with experimental data in the low-pressure regime ($P \leq 100$ kbar), with the following results (Sections 17-19 and 23 of [2]):

(a) Molecular dynamics (MD) calculations of the anharmonic contribution to the entropy of several solids match experimental entropy data to the accuracy of the data themselves.

(b) Low-temperature ($T \leq 20$ K) calculations of the electron-phonon term for several solids lead to predictions that also match experimental entropy to the accuracy of the data.

(c) Theoretical arguments show that the electron-phonon contribution is entirely negligible except when the electronic contribution dominates the free energy, such as in metallic solids at low temperatures.

(d) For the 27 elemental solids for which accurate data are available from low T (but not too low; see point (c)) to the melting temperature T_m, the free energy excluding the anharmonic and electron-phonon terms accounts for the experimental thermal energy and entropy to an accuracy of 5% (in fact, an accuracy of 2% for all but about five materials).

(e) For the 6 elements in the liquid phase for which accurate data are available at temperatures up to around $3\,T_m$, the effect of neglecting the anharmonic, boundary, and electron-phonon contributions to the energy and entropy is similarly small.

This tells us that at low pressures, we can neglect the anharmonic, boundary, and electron-phonon terms in both the solid and liquid free energy (which happen to be the hardest terms to calculate), and the resulting thermal energy and entropy are both simple in form and accurate at the 5% level. It is for this reason, not an appeal to the Born-Oppenheimer or other approximations, that we know we can simplify our EOS and what the results of the simplification will be, at least at low pressures.

In this paper we do two things: (1) We describe in more detail this framework for constructing EOS and discuss the theoretical and experimental inputs needed to implement it, and (2) we construct a sample EOS, neglecting anharmonic, boundary, and electron-phonon terms, both to illustrate the method and to discover whether points (d) and (e) above continue to hold in the high-pressure regime. We use Aluminum as our sample because of the availability of extensive electronic structure calculations, up to a compression of three, and highly accurate shock Hugoniot data, which provide a test of our EOS through both phases to pressures of around 5 Mbar. In Subsection 2.1 we develop the general theory of the solid EOS, and in Subsection 2.2 we do the same for the liquid. In Subsection 3.1, we construct our sample EOS for Al, comparing it with other EOS work, and in Subsection 3.2 we compute the Hugoniot predicted by the EOS and compare it with experimental data. The

results are encouraging. Finally, we review our work, discuss the advantages and disadvantages of this formalism (and how to address the disadvantages), and suggest directions for future development.

2 General theory

2.1 Solid phase

The condensed matter Hamiltonian, decomposed as described above, consists of terms describing the motion of the nuclei in a potential generated by the electrons in their ground state, plus additional terms that lead to the thermal excitation of the electrons and describe their interactions with the nuclear motion. With this Hamiltonian, the Helmholtz free energy per atom for a solid at temperature T with volume V per atom takes the form

$$F^{\mathrm{s}}(V,T) = \Phi_0^{\mathrm{s}}(V) + F_{\mathrm{ph}}^{\mathrm{s}}(V,T) + F_{\mathrm{el}}^{\mathrm{s}}(V,T) + F_{\mathrm{anh}}^{\mathrm{s}}(V,T) + F_{\mathrm{ep}}^{\mathrm{s}}(V,T). \quad (1)$$

Here Φ_0^{s} is the static lattice potential (the electronic ground state energy when the nuclei are fixed at their lattice sites); it depends on the particular crystal structure. $F_{\mathrm{ph}}^{\mathrm{s}}$ is the contribution from the harmonic motion of the nuclei about their lattice sites, $F_{\mathrm{el}}^{\mathrm{s}}$ represents the thermal excitation of the electrons when the nuclei are fixed at their lattice sites, $F_{\mathrm{anh}}^{\mathrm{s}}$ accounts for the anharmonicity of the nuclear motion (which may be represented as phonon-phonon interactions), and $F_{\mathrm{ep}}^{\mathrm{s}}$ expresses the interactions between the electron excitations and the nuclear motion, represented as electron-phonon interactions. (We emphasize again that this free energy is exact; it includes all of the physics present in the Hamiltonian.) The discussion in the Introduction justifies our approximating the solid free energy as

$$F^{\mathrm{s}}(V,T) = \Phi_0^{\mathrm{s}}(V) + F_{\mathrm{ph}}^{\mathrm{s}}(V,T) + F_{\mathrm{el}}^{\mathrm{s}}(V,T), \quad (2)$$

so let us now consider the forms of $F_{\mathrm{ph}}^{\mathrm{s}}$ and $F_{\mathrm{el}}^{\mathrm{s}}$ and the parameters on which they depend. The phonon term in the Hamiltonian describes harmonic motion, which leads uniquely to the free energy of lattice dynamics:

$$F_{\mathrm{ph}}^{\mathrm{s}}(V,T) = \int_0^{\infty} g^{\mathrm{s}}(\omega) \left[\frac{1}{2}\hbar\omega + \ln(1 - e^{-\beta\hbar\omega}) \right] d\omega, \quad (3)$$

where $\beta = 1/kT$ and $g^{\mathrm{s}}(\omega)$ is the distribution of phonon frequencies in the Brillouin zone. (Note that $g^{\mathrm{s}}(\omega)$ is volume dependent.) Sometimes we require

not the full Eq. (3) but only its high- and low-temperature limits, for which we need not the full $g^{\mathrm{s}}(\omega)$ but only three of its moments, expressed in terms of the characteristic temperatures Θ_0^{s}, Θ_1^{s}, and Θ_2^{s} defined by

$$
\begin{aligned}
\ln k\Theta_0^{\mathrm{s}} &= \langle \ln \hbar\omega \rangle_{\mathrm{BZ}} \\
k\Theta_1^{\mathrm{s}} &= \frac{4}{3}\langle \hbar\omega \rangle_{\mathrm{BZ}} \\
k\Theta_2^{\mathrm{s}} &= \left[\frac{5}{3}\langle (\hbar\omega)^2 \rangle_{\mathrm{BZ}}\right]^{1/2},
\end{aligned}
\tag{4}
$$

where $\langle \cdots \rangle_{\mathrm{BZ}}$ indicates an average over all the frequencies in the Brillouin zone. Then the following limits hold:

$$
F_{\mathrm{ph}}^{\mathrm{s}}(V, T) \rightarrow \frac{9}{8}k\Theta_1^{\mathrm{s}} \quad \text{as} \quad T \rightarrow 0
\tag{5}
$$

and

$$
F_{\mathrm{ph}}^{\mathrm{s}}(V, T) = -3kT \left[\ln\left(\frac{T}{\Theta_0^{\mathrm{s}}}\right) - \frac{1}{40}\left(\frac{\Theta_2^{\mathrm{s}}}{T}\right)^2 + \cdots\right] \quad \text{at high } T.
\tag{6}
$$

The leading term in Eq. (6) describes purely classical nuclear motion, while the series of terms in powers of T^{-2} are quantum corrections. Keeping only the first quantum correction, the thermodynamic functions derived from Eq. (6) are accurate to 1% at temperatures above $\frac{1}{2}\Theta_2^{\mathrm{s}}$.

The electronic excitation free energy $F_{\mathrm{el}}^{\mathrm{s}}$ can be expressed generally as an integral function of the electronic density of states per atom, $n^{\mathrm{s}}(\epsilon)$, and the Fermi distribution

$$
f(\epsilon) = \frac{1}{e^{\beta(\epsilon - \mu)} + 1},
\tag{7}
$$

where β is still $1/kT$ and μ is the chemical potential. If each atom contributes Z electrons to the valence bands (notice that Z is not necessarily the atomic number), with the lowest valence energy set to zero, then μ is a function of T determined by the normalization condition

$$
\int_0^\infty n^{\mathrm{s}}(\epsilon)f(\epsilon)\, d\epsilon = Z.
\tag{8}
$$

The electronic free energy is then

$$
\begin{aligned}
F_{\mathrm{el}}^{\mathrm{s}}(V, T) = \\
\mu Z - \int_0^{\epsilon_F} \epsilon\, n^{\mathrm{s}}(\epsilon)\, d\epsilon - kT \int_0^\infty n^{\mathrm{s}}(\epsilon) \ln[1 + e^{-\beta(\epsilon - \mu)}]\, d\epsilon,
\end{aligned}
\tag{9}
$$

5

where ϵ_F, the Fermi energy, is the value of μ when $T = 0$. The second term on the right hand side of Eq. (9) is the subtraction of the electronic ground state energy, which ensures that $F_{el}^s \to 0$ as $T \to 0$. This property makes sense if F_{el}^s represents purely thermal excitation of the electrons. (It also avoids double counting of the energy, as the electronic ground state energy is already represented as Φ_0^s.)

We see from this discussion that to evaluate the terms in Eq. (2) for the solid free energy we require three unknown functions: Φ_0^s, $g^s(\omega)$ (or Θ_0^s, Θ_1^s, and Θ_2^s if we are concerned only with the high- and low-T limits), and $n^s(\epsilon)$ (and the associated quantities Z and ϵ_F). These can be determined in various ways: compressibility data and diamond anvil cell data can be used to construct $\Phi_0^s(V)$; neutron scattering experiments can determine $g^s(\omega)$ or its various moments at $P = 1$ bar; and for many elements all three of these functions can be computed reliably using electronic structure theory. (Or one could use results from multiple sources in combination, which is often an option with Φ_0^s and is basically a necessity with $g^s(\omega)$.) One must keep in mind, however, that the accuracy of one's answers will be limited by the accuracy and range of applicability of these functions, regardless of how they are determined.

2.2 Liquid phase and two-phase region

According to the theory of liquid dynamics reviewed in [4], the same Hamiltonian that gave us the solid free energy leads to a similar form for the free energy of a monatomic liquid. In this theory, the region of the many-body potential surface in which the system moves in the liquid phase is dominated by a large number of intersecting nearly-harmonic valleys, called "random" valleys because they correspond to particle configurations which retain no remnant crystal symmetry, and which are all macroscopically identical. In particular, the valleys all have the same distribution of normal mode frequencies, and they all have the same depth (which, as in the solid case, is the electronic ground state energy when the nuclei are fixed at the valley minimum). The resulting liquid free energy per atom is

$$\begin{aligned} F^l(V,T) &= \Phi_0^l(V) + F_{ph}^l(V,T) + F_{el}^l(V,T) + F_{ab}^l(V,T) + \\ &\quad F_{ep}^l(V,T) - kT \ln w. \end{aligned} \tag{10}$$

All of the terms correspond to their solid counterparts with the following exceptions:

6

(1) Φ_0^l, now called the static *structure* potential, is the depth of a typical valley in which the liquid system moves.

(2) The normal mode spectrum appearing in F_{ph}^l is that of a typical liquid potential valley, not the unique solid potential valley.

(3) The term F_{ab}^l includes corrections due both to anharmonicity and to the fact that the potential valleys have boundaries, which the liquid (as opposed to the solid) encounters as it transits from valley to valley.

(4) The extra term $-kT\ln w$ corresponds to an increase in entropy of $k\ln w$ per atom; the value $\ln w \approx 0.8$ is estimated from entropy of melting data of the elements (again, see [4] for details). In liquid dynamics theory, this term is due to the hypothesis that the number of potential valleys among which the liquid moves is of order w^N, where N is the number of atoms in the system.

We emphasize that the same Hamiltonian gives rise to both Eq. (1) and (10); the differences are that the potential is expanded about different equilibrium configurations in the two cases, and that the region of configuration space over which the liquid moves is obviously far larger than the space available to the solid (hence the $-kT\ln w$ term).

Again making the approximations discussed in the Introduction, our form for the liquid free energy becomes

$$F^l(V,T) = \Phi_0^l(V) + F_{\text{ph}}^l(V,T) + F_{\text{el}}^l(V,T) - kT\ln w, \qquad (11)$$

and the additional term $-kT\ln w$ is fully determined by setting $\ln w = 0.8$, as mentioned above. The form of the phonon term is dictated by a central hypothesis of liquid dynamics theory: The motion of the liquid consists of oscillations in the macroscopically similar valleys described above together with occasional *transits* between valleys; the transits are of such short duration that they do not contribute to the thermodynamics to lowest order. Thus we will take F_{ph}^l to have the same form as the solid phonon term, Eq. (3), with a possibly different phonon frequency distribution $g^l(\omega)$. The electronic excitation term for the solid was derived using only the assumption that the electrons are thermally distributed over the available states using Fermi statistics; all of the information about the configuration of the nuclei is contained in the density of states. Hence F_{el}^l also takes the same form as the corresponding solid term, Eq. (9), with a density of states $n^l(\epsilon)$ appropriate for the liquid phase. (What this means is discussed briefly below.)

The liquid and solid EOS together determine the melting temperature as a function of pressure $T_m(P)$ by the requirement that the solid and liquid

Gibbs free energies match along the melt curve, or

$$G^{\text{s}}(P, T_m(P)) = G^l(P, T_m(P)). \tag{12}$$

Once the melt curve is determined, one can use the solid and liquid EOS separately to compute $V_m^{\text{s}}(T)$ and $V_m^l(T)$, the atomic volumes of the solid and liquid at melt as functions of temperature. (Of course, using $T_m(P)$ one can express V_m^{s} and V_m^l as functions of pressure equally well.)

In the case $V_m^{\text{s}}(T) < V_m^l(T)$ for all T, which we assume here, the computation of the full two-phase EOS (F, E, S, and P) for any V and T proceeds as follows. If $V \leq V_m^{\text{s}}(T)$ for the given T, the system is in the solid phase; F^{s} is computed as described in Subsection 2.1, and the other functions follow from

$$
\begin{aligned}
S^{\text{s}} &= -\left(\frac{\partial F^{\text{s}}}{\partial T}\right)_V, \\
E^{\text{s}} &= F^{\text{s}} + T S^{\text{s}}, \\
P^{\text{s}} &= -\left(\frac{\partial F^{\text{s}}}{\partial V}\right)_T.
\end{aligned}
\tag{13}
$$

If $V \geq V_m^l(T)$, the system is in the liquid phase; F^l is computed as described in this Subsection, and the other functions follow from expressions analogous to Eqs. (13). If $V_m^{\text{s}}(T) < V < V_m^l(T)$, the system is in the two-phase region; defining η, the volume fraction of the system in the liquid phase, by

$$\eta = \frac{V - V_m^{\text{s}}(T)}{V_m^l(T) - V_m^{\text{s}}(T)}, \tag{14}$$

the thermodynamic functions are

$$
\begin{aligned}
F(V,T) &= \eta\, F^l(V_m^l(T), T) + (1 - \eta) F^{\text{s}}(V_m^{\text{s}}(T), T), \\
E(V,T) &= \eta\, E^l(V_m^l(T), T) + (1 - \eta) E^{\text{s}}(V_m^{\text{s}}(T), T), \\
S(V,T) &= \eta\, S^l(V_m^l(T), T) + (1 - \eta) S^{\text{s}}(V_m^{\text{s}}(T), T), \\
P(V,T) &= -\frac{F^l(V_m^l(T), T) - F^{\text{s}}(V_m^{\text{s}}(T), T)}{V_m^l(T) - V_m^{\text{s}}(T)}.
\end{aligned}
\tag{15}
$$

Finally, we note that just as with the solid, to evaluate the terms in Eq. (11) we require three unknown functions: Φ_0^l, $g^l(\omega)$ (or Θ_0^l and Θ_2^l, since we're not likely to need the low-T limit), and $n^l(\epsilon)$. In contrast to the solid case,

these functions are generally not available experimentally. (It is possible that one might be able to compute Φ_0^l using liquid compressibility data, but we suspect that this will be very difficult.) However, for many materials these functions should be computable using electronic structure theory, proceeding much as one would in the solid case except that the nuclei would be arranged not in a crystal configuration but in a disordered structure characteristic of a "random" valley in the liquid potential surface [4]. To our knowledge very few such calculations have been attempted; the only ones we are aware of are Φ_0^l and $g^l(\omega)$ at a single volume for liquid sodium in [5] (the results are referred to in [4] and a graph of $g^l(\omega)$ using their results appears as Fig. 1 in [6]). Another function that is sometimes available is the melt curve $T_m(P)$, but this curve cannot be chosen independently of the others, since the solid and liquid EOS determine it jointly; but this can be an advantage, since if $T_m(P)$ is known from experiment, for example, it can be used to compute one of the other needed functions if it is not otherwise available. In fact, this is how we will determine Φ_0^l in our example EOS, to which we now turn.

3   An example: Aluminum

To illustrate the application of the theory we've described, we will now construct an EOS for Aluminum, which has been the subject of extensive electronic structure calculations and for which a great deal of high-quality experimental data are available. We will then compare the Hugoniot predicted by our EOS with data up to pressures of approximately 5 Mbar; this will tell us whether the approximations we discussed in the Introduction (neglecting anharmonic, boundary, and electron-phonon effects), known to be accurate at low pressures, continue to be reasonable in the high-pressure domain.

3.1   Constructing the EOS

We recall from Subsection 2.1 that the solid EOS requires three functions: Φ_0^s, $g^s(\omega)$, and $n^s(\epsilon)$. Since we will be testing the EOS by comparison with Hugoniot data, we will always be in the high-T region (except for one brief low-T excursion; see below), so we use Eq. (6) for F_{ph}^s instead of Eq. (3); this means that we require only Θ_0^s, Θ_1^s, and Θ_2^s in place of $g^s(\omega)$.

To determine these functions, we began by consulting the results of density functional theory (DFT) calculations carried out in the local density ap-

proximation by Straub et al. [7]. They worked with fcc and bcc Al at atomic volumes from 37 a_0^3 to 160 a_0^3, where a_0 is the Bohr radius, corresponding to densities from 8.17 g/cm³ to 1.89 g/cm³ (the density of Al at 293 K and 1 bar is 2.700 g/cm³). Their calculations indicate a $T = 0$ transition from fcc to bcc at 51 a_0^3, corresponding to $\rho = 5.93$ g/cm³, but we will neglect this phase change and treat solid Al as an fcc crystal for two reasons: The DFT calculations themselves suggest that the effect of the phase change on the thermodynamic functions will be quite small; and we know from experiment that the solid-liquid transition on the Hugoniot takes place well before reaching the density of concern (see Subsection 3.2), so we are confident of our assumption of fcc along the Hugoniot until melting. However, this assumption may have an effect on the liquid EOS at high densities, which we will comment on below. (Other electronic structure work, discussed on pp. 89-90 of [8], suggests the possibility of an hcp phase between the fcc and bcc phases, but as [8] also mentions, no experimental signature of this phase has been found, so we will proceed under the assumption of a single solid phase.)

Straub et al. computed Φ_0^s for fcc by fitting their results to a Birch-Murnaghan form,

$$\Phi_0^s(V) = c_0 + V_b \sum_{n=2}^{5} \frac{c_n}{n!} \left\{ \frac{1}{2} \left[\left(\frac{V}{V_b} \right)^{-2/3} - 1 \right] \right\}^n , \qquad (16)$$

with coefficients

$$
\begin{aligned}
V_b &= 106.302 \, a_0^3, & c_0 &= -287.7832 \text{ mRy}, \\
c_2 &= 761.2029 \text{ GPa}, & c_3 &= 1319.036 \text{ GPa}, \\
c_4 &= -13\,661.06 \text{ GPa}, & c_5 &= 50\,315.53 \text{ GPa}.
\end{aligned}
\qquad (17)
$$

The Θ_n^s were determined by computing the bulk modulus and four zone-boundary phonons at several volumes, and these results were used to calibrate a pseudopotential model at each volume. The pseudopotential was then used to calculate phonon frequencies throughout the Brillouin zone, allowing the determination of Θ_0^s, Θ_1^s, and Θ_2^s. Their results are shown in Table 1 and Figure 1. (The full set of results was not reported in [7].) To check these results, Straub et al. compared experimental phonon moments for Al at $T = 80$ K and $P = 1$ bar based on Born-von Karmen fits to neutron scattering data [9] with their predictions interpolated to the appropriate atomic volume of 110.7 a_0^3. The experimental points, also shown in Figure 1, are in very

V (a_0^3)	Θ_0^s (K)	Θ_1^s (K)	Θ_2^s (K)
111.97	278.09	386.55	387.20
106.65	304.63	423.81	424.86
93.318	381.43	532.00	534.48
74.655	525.01	735.49	741.68
55.991	741.62	1044.7	1058.3
37.327	1109.5	1575.0	1605.4

Table 1: DFT calculations of Θ_0^s, Θ_1^s, and Θ_2^s from [7].
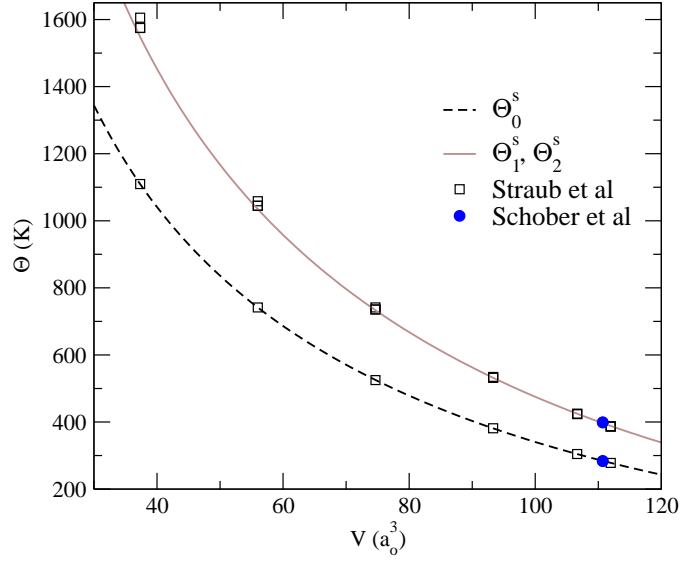
Figure 1: Θ_0^s, Θ_1^s, and Θ_2^s as functions of atomic volume from the DFT calculations in [7] and experimental data from [9]. Our functional forms are also shown.

good agreement with their calculations; hence these results for the Θ_n^{s} are acceptable for use in our EOS without modification. To determine the Θ_n^{s} at any volume, we first constructed a functional fit to the Θ_0^{s} points, with the result

$$\Theta_0^{\mathrm{s}}(V) = 2852.69 + \frac{17\,319.9}{V} + 2.33667\,V - 633.858\ln(V), \qquad (18)$$

where Θ_0^{s} is in K and V is in a_0^3. Then we noted that according to the DFT results both Θ_1^{s} and Θ_2^{s} approximately equal $e^{1/3}\,\Theta_0^{\mathrm{s}}$, so we made the same approximation using Eq. (18) for Θ_0^{s} to determine Θ_1^{s} and Θ_2^{s} at any volume. These functions are also shown in Figure 1.

The DFT calculations also provided data on the electronic density of states $n^{\mathrm{s}}(\epsilon)$. Graphs of $n^{\mathrm{s}}(\epsilon)$ for fcc and bcc Al at atomic volume 112.0 a_0^3 (corresponding to $P = 0$ and $T = 295$ K) are shown in Figure 2, along with the free electron $n^{\mathrm{s}}(\epsilon)$, for which

$$n^{\mathrm{s}}(\epsilon) = \sqrt{\frac{\epsilon}{\epsilon_F}} \left(\frac{3Z}{2\epsilon_F} \right) \qquad \text{and} \qquad \epsilon_F = \frac{\hbar^2}{2m_e} \left(\frac{3\pi^2 Z}{V} \right)^{2/3}, \qquad (19)$$

at $V = 112.0\,a_0^3$ and $Z = 3$. The Figure shows that the free electron model is a good approximation for either crystal structure, for electronic excitations to around $\frac{1}{2}$ Ry. The same match, at a slightly poorer level of approximation and for excitations to around 1 Ry, is found at our smallest atomic volume of 37 a_0^3. For all volumes of our study and temperatures up to T_m, the total electronic excitation contribution to the energy, entropy, and pressure is at most 5%, so the error introduced by using the free electron $n^{\mathrm{s}}(\epsilon)$ in our calculations is negligible. Making this approximation, the normalization condition from Eq. (8) becomes

$$F_{1/2}(\beta\mu) = \frac{2}{3}(\beta\epsilon_F)^{3/2}, \qquad (20)$$

which determines μ as a function of V and T, and Eq. (9) for the free energy becomes

$$F_{\mathrm{el}}^{\mathrm{s}}(V,T) = Z \left(\mu - \frac{2}{3}\,kT\,\frac{F_{3/2}(\beta\mu)}{F_{1/2}(\beta\mu)} - \frac{3}{5}\epsilon_F \right) \qquad (21)$$

where $Z = 3$. The $F_n(x)$ are the standard Fermi integrals; their properties are discussed on pp. 332-334 of [10] and their values for various n are tabulated in [11, 12].
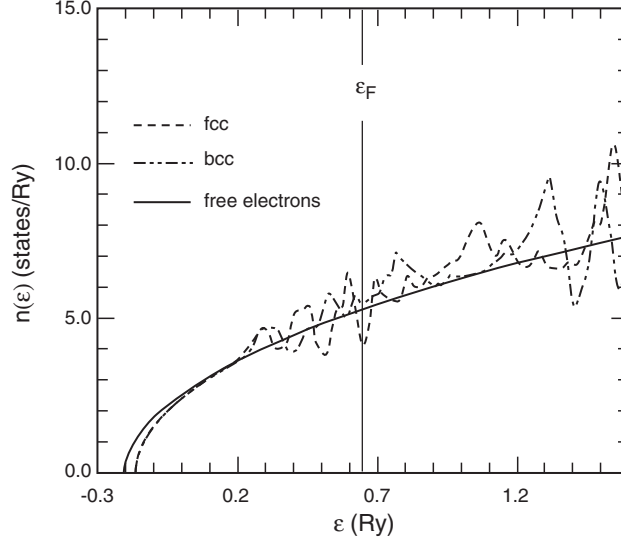
12

Figure 2: $n^s(\epsilon)$ for bcc and fcc Al at atomic volume 112.0 a_0^3 from the calculations in [7]. The free electron $n^s(\epsilon)$ at this volume and $Z = 3$ from Eq. (19) is shown for comparison. (From [2].)

The solid EOS that results from assembling all of these functions is reliable over a large range of volumes and temperatures; however, it is not in perfect agreement with the highly accurate experimental data that are available at low pressures. Specifically, experiments on Al at $T = 0$ and $P = 0$ show that [7]

$$V_0 = 110.6 \ a_0^3, \qquad E_0 = -249 \ \mathrm{mRy},$$
$$B_0 = 79.4 \ \mathrm{GPa}, \qquad \frac{dB_0}{dP} = 4.7, \tag{22}$$

but the EOS yields $V_0 = 107.3 \ a_0^3$, which is outside the experimental error. Therefore, we chose to make a small correction to our purely theoretical free energy to agree with experiment. These quantities are obviously determined by the $T = 0$ form of the free energy, $F_0^s = \Phi_0^s + \frac{9}{8}k\Theta_1^s$ (see Eq. (5)); since Θ_1^s is already in excellent agreement with available experiment, we chose to modify only Φ_0^s. To proceed, we noted that the data determine P_0, the $T = 0$ pressure, in the vicinity of $V = V_0$ by the relation

$$P_0(V) \;\; = \;\; P_0(V_0) + \left.\frac{dP_0}{dV}\right|_{V_0} (V - V_0) + \frac{1}{2}\left.\frac{d^2 P_0}{dV^2}\right|_{V_0} (V - V_0)^2 + \cdots$$

13

$$= -\frac{B_0}{V_0}(V - V_0) + \frac{B_0}{2V_0^2}\left(1 + \frac{dB_0}{dP}\right)(V - V_0)^2 + \cdots \qquad (23)$$

while at higher compressions we have no information to supplement the electronic structure result; so we decided to construct a Φ_0^s that correctly reproduces Eq. (23) near V_0 but smoothly interpolates to Eq. (16) at lower volumes. To do this, we computed P_0 at 10 volumes between 110 a_0^3 and 111.25 a_0^3 using Eq. (23), and we also computed $P_0 = -\partial F_0^s/\partial V$ using the above form for F_0^s, with Φ_0^s from Eq. (16), at 23 volumes between 30 a_0^3 and 41 a_0^3. We then performed a least-squares fit to these points using an expression similar to the Birch-Murnaghan form, but carried to a slightly higher order; after integrating, adjusting the constant of integration to correctly match E_0 from Eq. (22), and subtracting off $\frac{9}{8}k\Theta_1^s$, we had a new Φ_0^s given by

$$
\begin{aligned}
\Phi_0^s(V) \;=\; & -1.64615 \times 10^6 + \frac{2.07608 \times 10^7}{V^{2/3}} - \frac{4.61515 \times 10^8}{V^{4/3}} \\
& + \frac{5.71249 \times 10^9}{V^2} - \frac{5.49998 \times 10^{10}}{V^{8/3}} + \frac{3.71978 \times 10^{11}}{V^{10/3}} \\
& - \frac{1.66284 \times 10^{12}}{V^4} + \frac{4.41118 \times 10^{12}}{V^{14/3}} - \frac{5.25064 \times 10^{12}}{V^{16/3}} \\
& + \frac{2.26789 \times 10^7}{V} - 220.716\,V + 23\,6788\ln(V) \qquad (24)
\end{aligned}
$$

where Φ_0^s is in mRy and V is in a_0^3. This Φ_0^s, which reproduces the data in Eq. (22) and interpolates smoothly to the DFT curve at higher compressions, is what we use in our EOS instead of Eq. (16). The $T = 0$ pressure-volume curves constructed using both the original and new Φ_0^s are shown in Figure 3.

Our choice of a Birch-Murnaghan-like form was dictated by the fact that the Straub et al. result provides most of our information about the shape of Φ_0^s; so our goal was to preserve that form insofar as was possible, interpolating back to their result as quickly as we could without introducing enough curvature to compromise agreement with dB_0/dP. This correction to Φ_0^s constitutes a small change to the overall EOS; the effect of this change on the Hugoniot will be considered in the next Section. This modification completes the full solid free energy, so we can now consider the liquid.

For the liquid we need the same three functions that we needed for the solid, and we must also consider the melting curve $T_m(P)$. Having chosen to
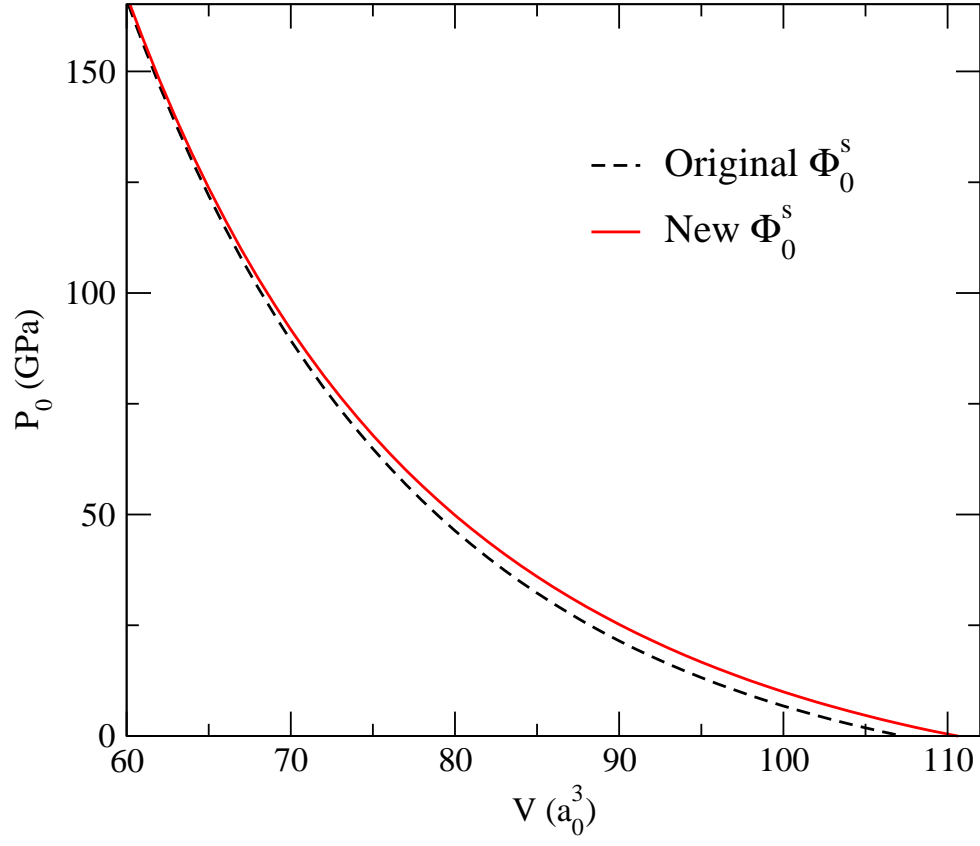
Figure 3: The $T = 0$ pressure-volume relations calculated using the original Φ_0^s and the new Φ_0^s we constructed. Notice how they differ in the vicinity of $V = 110.6\ a_0^3$ but then agree more closely at lower volumes.

use Eq. (6) for $F_{\mathrm{ph}}^{\mathrm{s}}$, we certainly did the same for F_{ph}^l, since the Hugoniot will obviously enter the liquid region only at rather high temperatures; thus we needed only Θ_0^l and Θ_2^l. From experiment we know that Al is what is called in liquid dynamics a "normal melting element" (the entropy of melting at constant density is approximately $0.8\,k$ per atom), and we argue in [4] that Θ_0 in solid and liquid phases of such an element are approximately equal. (Experimental and computational work supporting this conjecture are also discussed in [4].) Thus we took the liquid to have the same Θ_0 as the solid. It is also true that in the liquid, T is typically much larger than Θ_2^{s} (for example, in liquid Al at normal density $T \geq 2\Theta_2^{\mathrm{s}}$), rendering the first quantum correction to F_{ph}^l negligible (roughly 1% at normal density), so even if Θ_2^l differs from Θ_2^{s} by 25% or more, the impact on the phonon term will be very small; therefore we also used the same Θ_2 in the liquid as in the solid.

Since the free electron model approximates the DFT result for $n^{\mathrm{s}}(\epsilon)$ so well for both fcc and bcc Al (Figure 2), which correspond to two valleys in the many-body potential surface with rather different structures, we also expect this model to be a good approximation for $n^l(\epsilon)$, the density of states for the structure characteristic of a liquid. Since at all volumes and temperatures up to $5\,T_m$ (the relevance of this number will appear below), the electronic contribution to the thermodynamic functions does not exceed 25%, the error introduced by the free electron model is still acceptable.

We fixed the only remaining term in Eq. (11), Φ_0^l, by the requirement that the Gibbs free energies of the solid and liquid match along the Al melting curve. Boehler and Ross [13] suggested that

$$T_m(P) = 933.45 \text{ K} \left(\frac{P}{6.049 \text{ GPa}} + 1 \right)^{0.531} \tag{25}$$

on the basis of their experimental work up to 80 GPa (0.8 Mbar), and experiments by McQueen et al. [14] and Hänström and Lazor [15] and theoretical work by Pélissier [16] suggest that this curve continues to be accurate up to 200 GPa. In the absence of evidence to the contrary, we took Eq. (25) to be valid to higher pressures as needed. (As we will see later, our EOS will assume Eq. (25) no higher than 400 GPa.) We computed Φ_0^l as follows: We made a guess for Φ_0^l not very different from Φ_0^{s}, and then we used it and Eq. (25) to calculate the difference between the two Gibbs free energies,

$$\Delta G(P) = G^{\mathrm{s}}(P, T_m(P)) - G^l(P, T_m(P)), \tag{26}$$

16

at several hundred values of P over the entire pressure range considered in this study. We also calculated the liquid melt volume $V_m^l(P)$ at each P. If the rms average of Eq. (26) over all calculated points was not sufficiently small, we used the following easily verified fact: To first order, a small change $\delta\Phi_0^l$ produces a small change $\delta G^l(P, T_m(P))$ given by $\delta G^l(P, T_m(P)) = \delta\Phi_0(V_m^l(P))$. Thus we performed the substitution

$$\Phi_0^l(V) \rightarrow \Phi_0^l(V) + \Delta G(P_m^l(V)), \qquad (27)$$

where ΔG was computed by Eq. (26) and $P_m^l(V)$ is the inverse of $V_m^l(P)$, and calculated Eq. (26) again. We iterated until the rms average was sufficiently small (less than 0.001 mRy in our case), giving us the needed Φ_0^l, which is shown in Figure 4 along with Φ_0^s. We recorded Φ_0^l as a list of points, and we did not create a functional fit for it; instead we used an interpolator to calculate it and its derivative when needed.

It is at this point that the existence of other solid phases in Al, discussed earlier, affects the EOS of the liquid. It is likely that the liquid region borders the fcc crystal only over part of its boundary, beyond which the liquid borders the bcc region or other solid phases. In such a case, at sufficiently high pressures we should use the free energy appropriate for that solid phase, not the fcc free energy, in Eq. (26). This suggests that Φ_0^l may become inaccurate beyond densities in the neighborhood of 6 g/cm^3, where the $T = 0$ fcc-bcc phase transition occurs. We will take this fact into consideration when we discuss the limits of applicability of the EOS below.

Once we had the full solid and liquid EOS, we then solved Eq. (12) directly to compute $T_m(P)$, verifying that we had reproduced the Boehler-Ross curve; our result is shown in Figure 5, together with the data from [14, 15] and some points from Pélissier's theoretical curve. (According to [14], their data point at 125 GPa marks the onset of melting along the Hugoniot. We will comment on this in the next Subsection.)

Now that we have the full two-phase EOS, it is profitable to compare our work with another EOS for Al, due to Moriarty et al. [17]. These authors also use a full lattice dynamics treatment of the crystal phonons, although they calculate their $g^s(\omega)$ two separate ways, using both Moriarty's Generalized Pseudopotential Theory (GPT) and a local pseudopotential model with parameters chosen to match solid-phase EOS data. We strongly prefer to rely on DFT results, as we believe DFT has reached such a stage of maturity that it more accurately captures the physics contained in the real Hamiltonian of the system, which as we have emphasized we believe to be understood
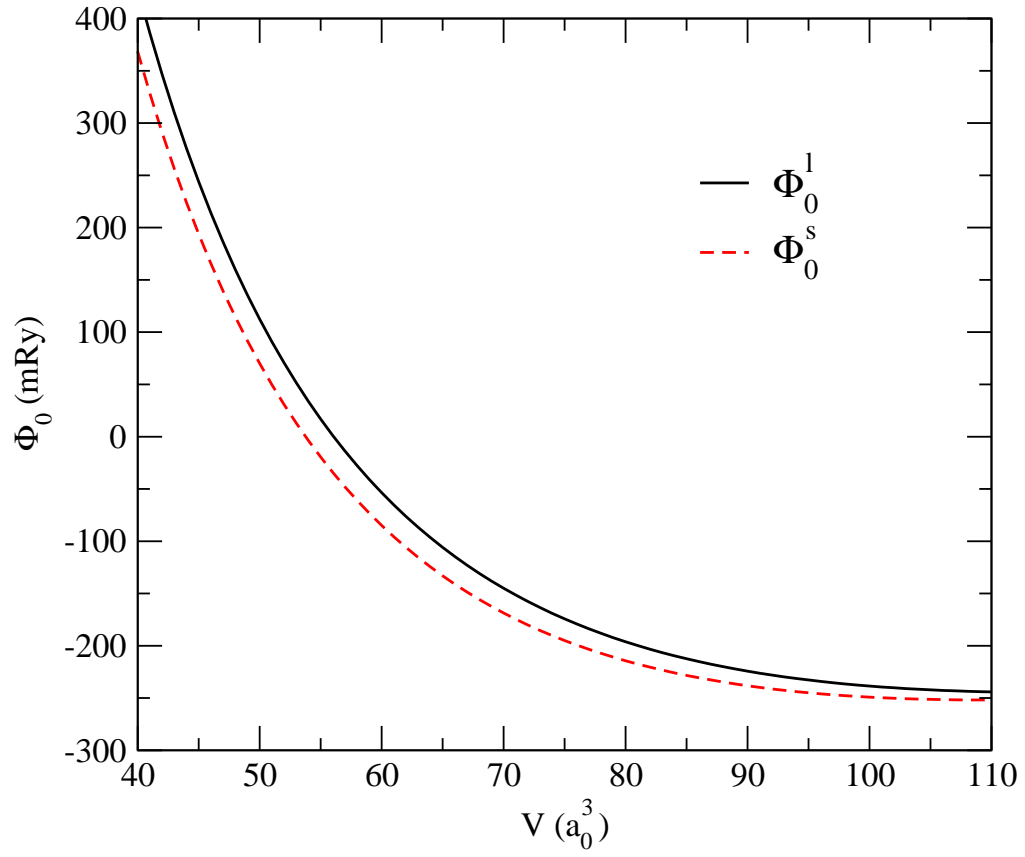
17

Figure 4: Φ_0^l determined by matching the liquid and solid Gibbs free energies along the melt curve. Φ_0^s is also shown for comparison.
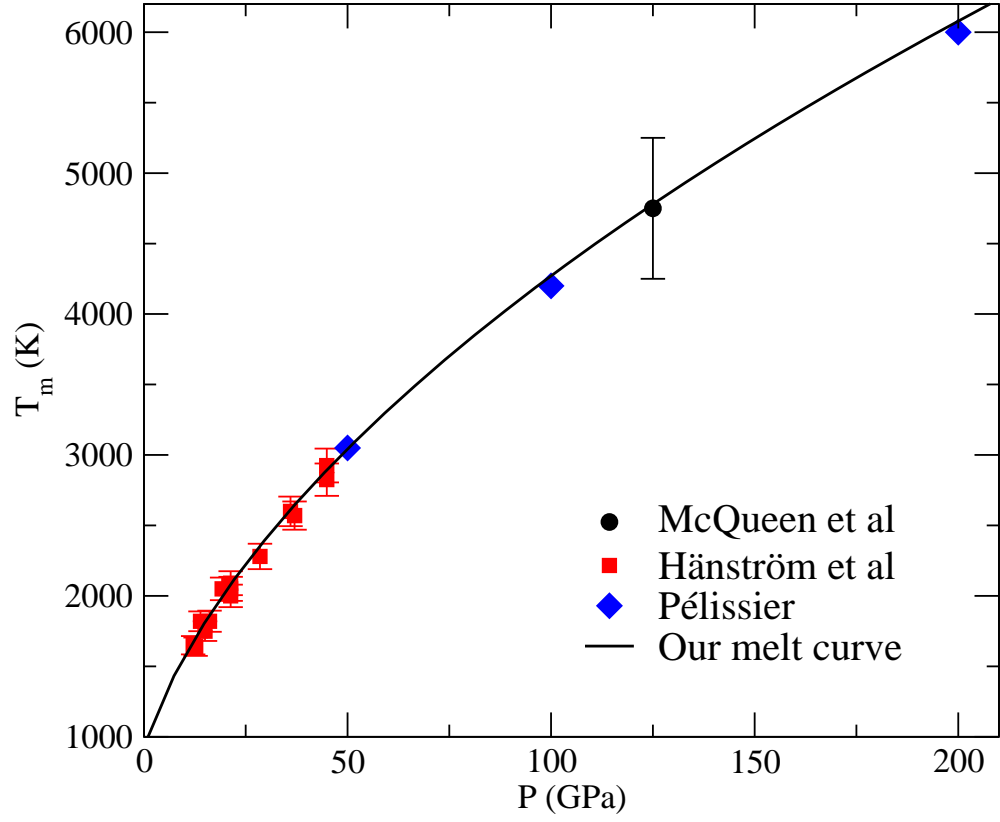
Figure 5: The melt curve $T_m(P)$ computed from our full solid and liquid EOS (which reproduces the Boehler-Ross curve, Eq. (25)), the experimental data from [14, 15], and points from the theoretical curve in [16].

in sufficient depth that it should underlie all of our work. Second, in their treatment of the liquid phase Moriarty et al. rely on fluid variational theory, described in detail in [18], to compute the least upper bound to the "real" liquid free energy (from a liquid Hamiltonian based on pseudopotentials) that can be obtained from the free energy of a reference system; Moriarty et al. investigate hard-sphere, soft-sphere, and one-component plasma reference systems before settling on the soft-sphere system as providing the best bound. Based on the investigations summarized in [4], we claim that we have the actual Hamiltonian of the liquid itself, not a Hamiltonian based on pseudopotential theory; furthermore, this Hamiltonian decomposes naturally into a dominant term that produces a free energy that can be used directly (instead of requiring approximation by the free energy of a reference system) and remaining terms whose contributions to the free energy are known to be small (see the Introduction). The same point we made above for the solid phase applies; we argue that it is a better strategy in developing EOS to try to understand the true Hamiltonian of the system, and then to use it when doing statistical mechanics. Almost inevitably, one must make approximations (which we certainly have done here), but we believe we are in a better position to understand and improve upon them if the physical foundation of the EOS is as solid as we can make it.

Finally, let us make some conservative estimates of the range of applicability of this EOS. Any limits will arise from two sources: the validity of the approximation that F^l_{ab} is negligible in the liquid (see the Introduction), and the limited ranges over which the functions $\Phi_0(V)$, $g(\omega)$, $n(\epsilon)$, and $T_m(P)$ are known. Let's consider each in turn.

(1) We know from experiment that F^l_{ab} is negligible when $T \leq 3\,T_m$ (again, see the Introduction), and judging from trends in the data we suspect F^l_{ab} will still be small up to $T \approx 5\,T_m$, but clearly this term must become relevant as the nuclear motion becomes more gaslike. Thus we shall take care with any data at ρ and T such that T approaches or exceeds $5\,T_m(\rho)$.

(2) At densities below approximately 6 g/cm^3, we are confident that the solid is in the fcc phase, and the liquid free energy is based on this phase, so we trust the full EOS here. At higher densities, we must be more circumspect; the solid may have undergone a phase transition to bcc, and the liquid EOS at this density may be based on the wrong solid free energy. Further, as we have indicated earlier, Eq. (25) for the melt curve has received independent support only up to 200 GPa, so we must be cautious with the liquid EOS in regions beyond this point. We decided to be brave and accept the

melt curve as valid up to 400 GPa; this corresponds to a liquid density of 6.15 g/cm^3, and since this is not far from the probable location of the solid fcc-bcc transition, we take it as the density limit of our EOS. (Even if we did not have this concern, we would be restricted to densities below 8.17 g/cm^3, where electronic structure results are available.) Also, the free electron approximation to $n^s(\epsilon)$ has been validated only for $\epsilon - \epsilon_F$ up to 1/2 Ry, or 6.8 eV, at low compression and 1 Ry, or 13.6 eV, at high compression, but at higher temperatures the electronic energy and entropy are sensitive to the details of $n^s(\epsilon)$ to energies above these limits. We estimated the values of T that begin to probe the unvalidated region of $n^s(\epsilon)$ (roughly $3kT = \epsilon - \epsilon_F$), and we found that over our valid density range the $T = 5\,T_m$ limit always took precedence. Hence this limit is not relevant for us, but we mention it for completeness, as it may become a concern if the EOS is extended to higher densities.

Figure 6 shows the limits $\rho \leq 6.15$ g/cm^3 and $T \leq 5\,T_m$ of the EOS in $T - P$ space, together with the melt curve and the Hugoniot (see the next Subsection), while Figure 7 shows the same three features in $T - \rho$ space. In this Figure, the melt curve becomes a two-phase region, which we will consider in more detail in the next Subsection. We are confident that this EOS is valid within these limits, but we don't know how far beyond them the inaccuracies begin to appear; thus we will not be shy about considering data not too far outside this range.

3.2   Comparison with Hugoniot data

If a shock wave travels at speed u_s through a sample of material, accelerating its particles from rest to speed u_p and changing its density, atomic volume, pressure, and internal energy per atom from ρ_0, V_0, P_0, and E_0 to ρ, V, P, and E, then (assuming thermal equilibrium before and after the shock) these quantities must satisfy the Rankine-Hugoniot relations,

$$
\begin{aligned}
\rho(u_s - u_p) &= \rho_0 u_s \\
P - P_0 &= \rho_0 u_s u_p \\
E - E_0 &= \frac{1}{2}(P_0 + P)(V_0 - V),
\end{aligned}
\tag{28}
$$

derived from considerations of mass, momentum, and energy conservation. (It is assumed that the wave is steady and strength effects are negligible.)
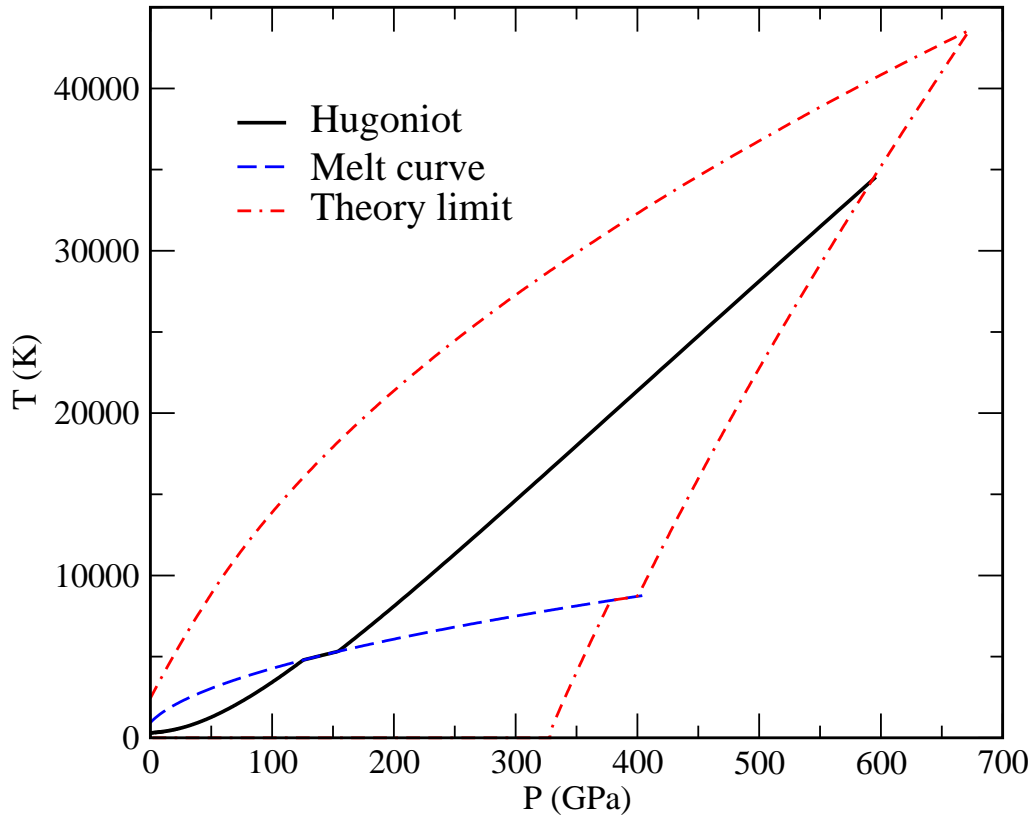
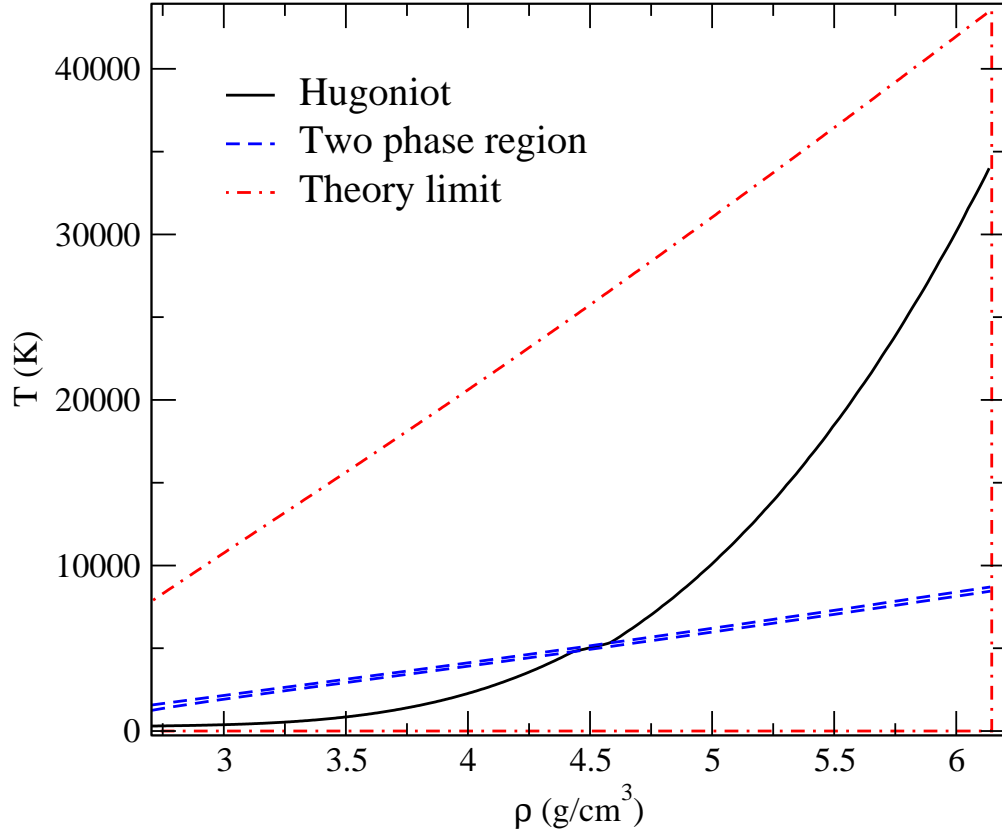Figure 6: The limits of our EOS, the melt curve, and the Hugoniot.

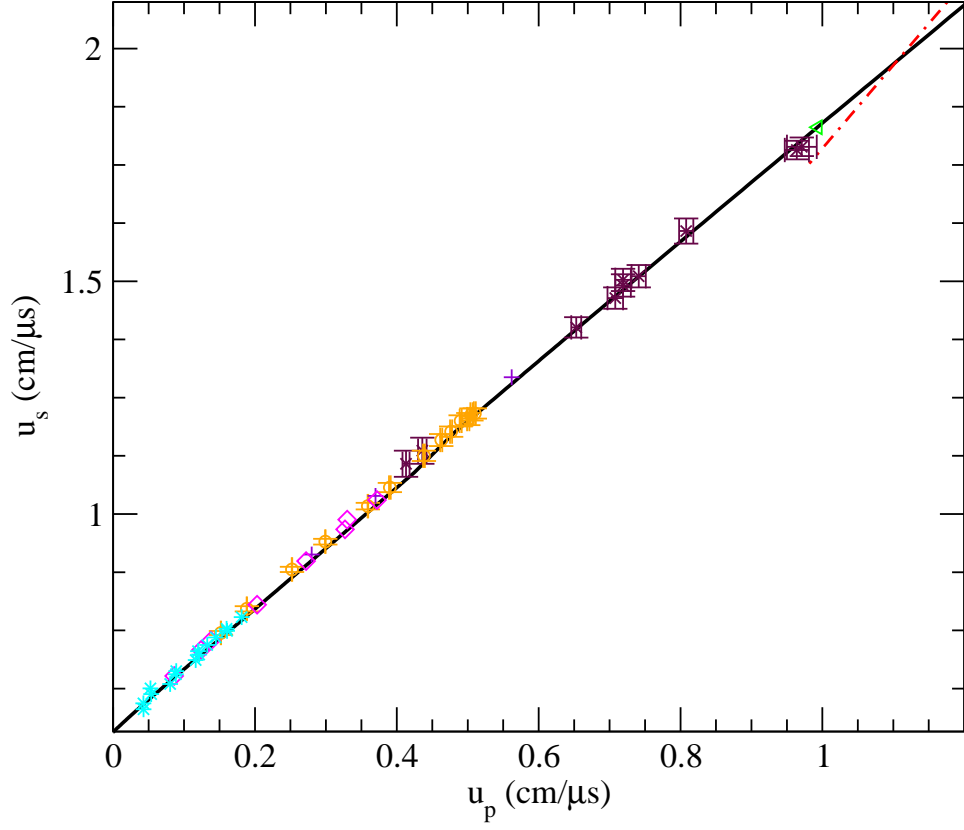Figure 7: The limits of our EOS, the two-phase region (solid below the region, liquid above), and the Hugoniot.

Figure 8: The u_s-u_p Hugoniot for Al predicted by our EOS together with experimental data from [19, 20, 21, 22, 23, 24]. The intersection of the Hugoniot with the limit of validity of the EOS (dot-dash line) is also indicated.
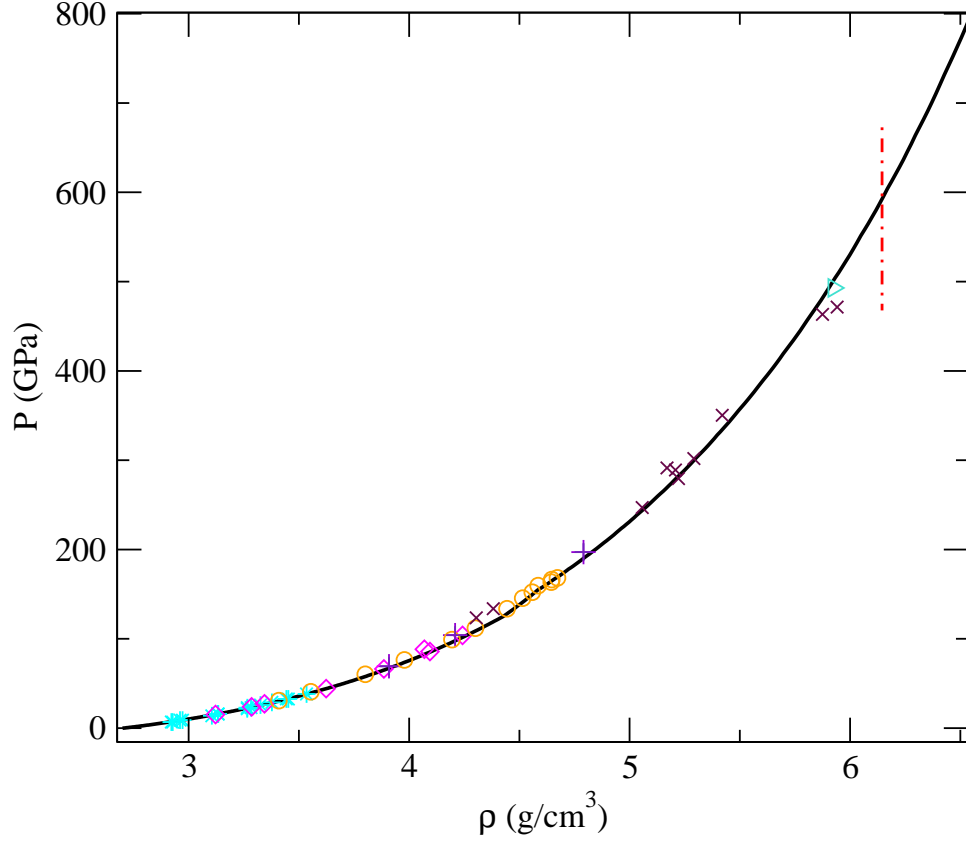
Figure 9: The P-ρ Hugoniot for Al predicted by our EOS together with experimental data from [19, 20, 21, 22, 23, 24]. The intersection of the Hugoniot with the limit of validity of the EOS (dot-dash line) is also indicated.

By solving these equations together with the EOS, which relates P, V, and E, we can determine the Hugoniot, the curve of all possible end states of the shocked material. We used our EOS and Eqs. (28) to compute u_s as a function of u_p and P as a function of ρ along the Al Hugoniot; the results are shown in Figures 8 and 9 along with the intersection of the Hugoniot with the limit of validity of the EOS. Hugoniot data from several sources [19, 20, 21, 22, 23, 24] are also included. The low-pressure region of the Hugoniot is highlighted in Figures 10 and 11, and the intermediate-pressure region, including the intersections with the phase boundaries, is shown in Figures 12 and 13.
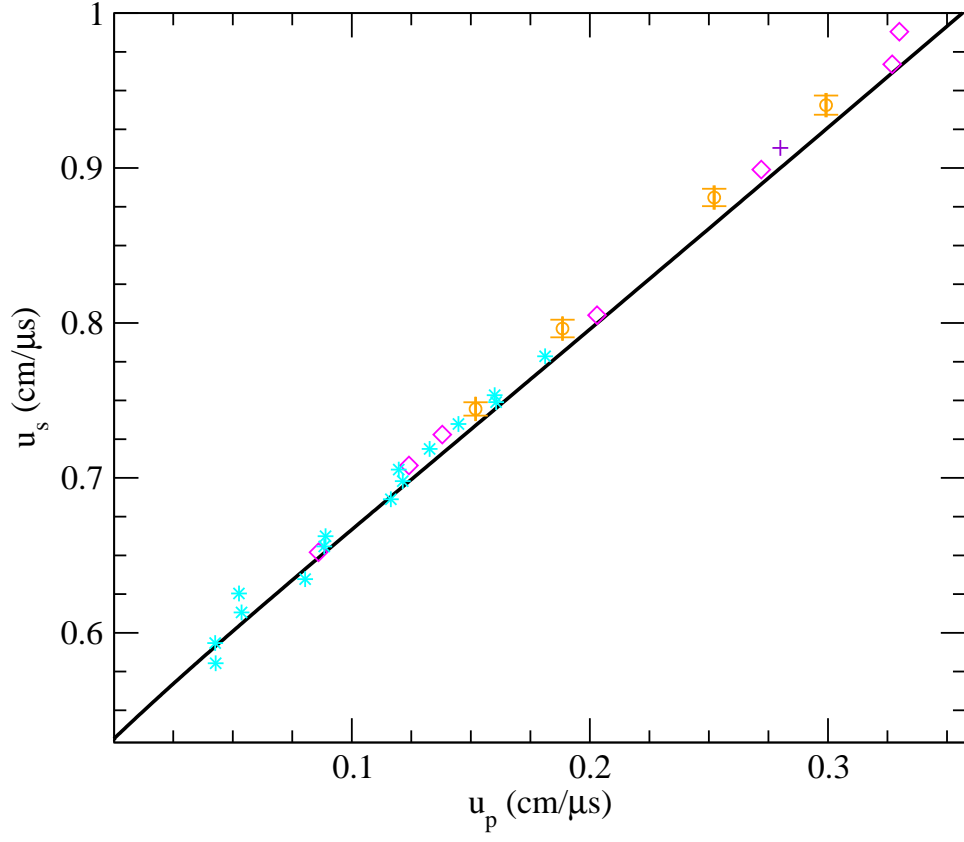
Figure 10: The u_s-u_p Hugoniot in the low-P region, with data from [19, 21, 22, 23]. The u_p error bars on the circles [23] appear as slightly broadened vertical lines.
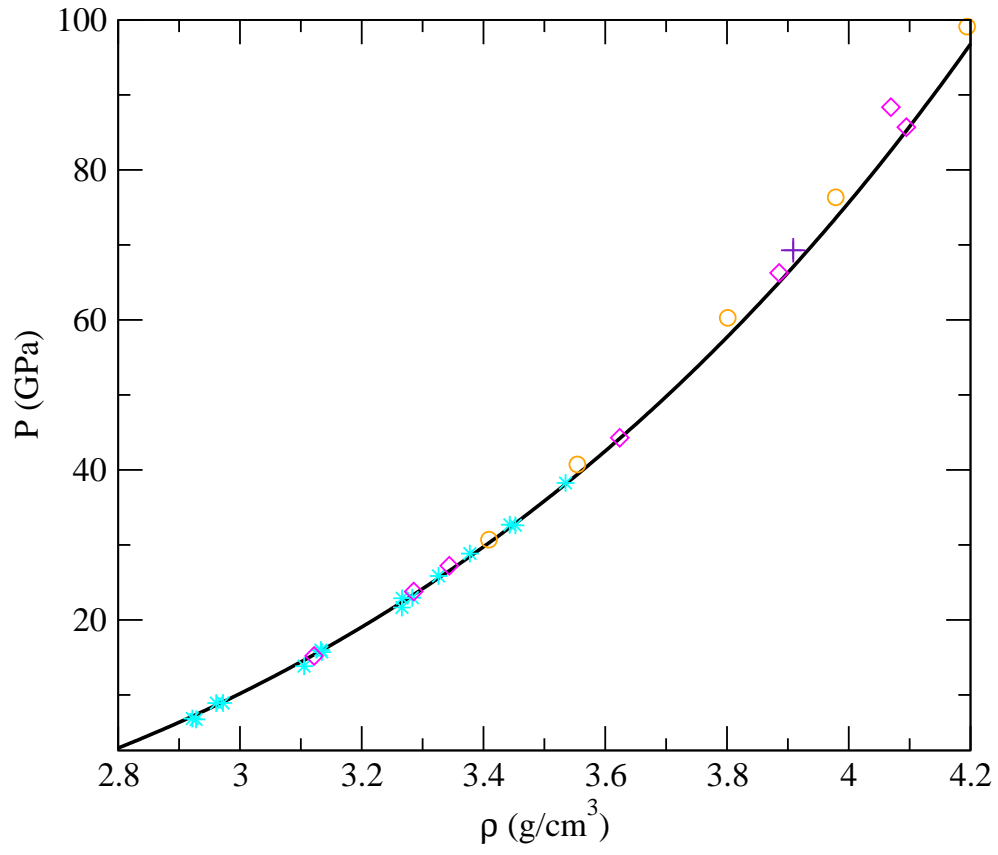
Figure 11: The P-ρ Hugoniot in the low-P region, with data from [19, 21, 22, 23].
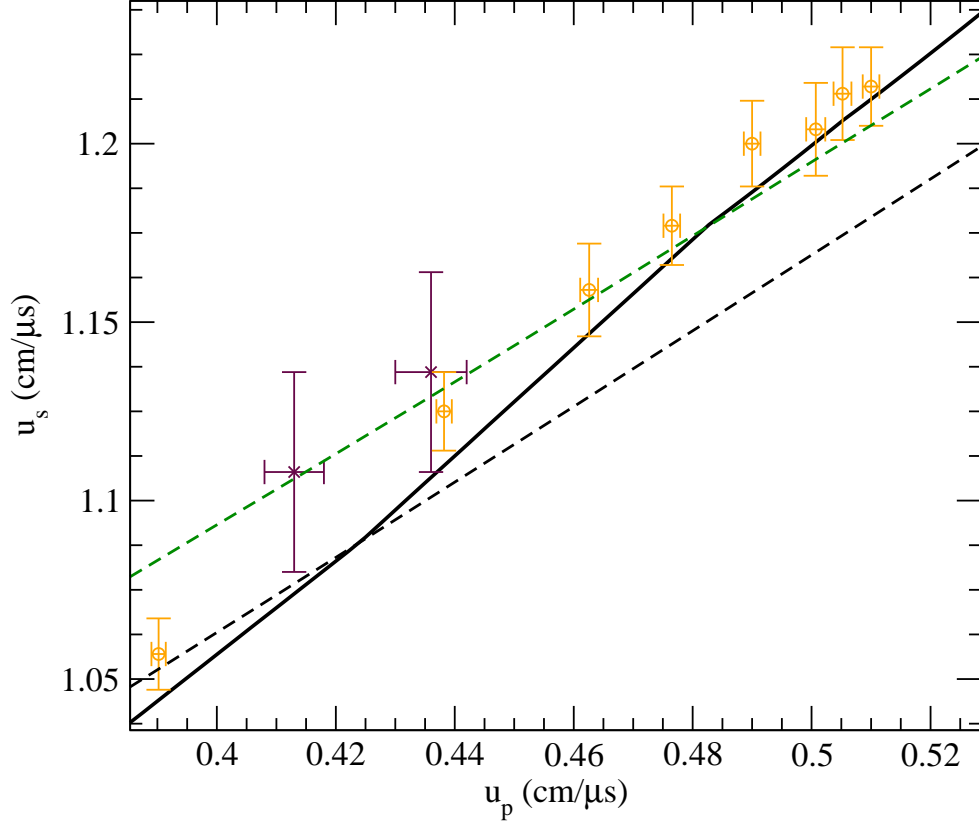
Figure 12: The u_s-u_p Hugoniot in the intermediate-P region, including intersections with the phase boundaries, with data from [23, 24].

Three important considerations in selecting which data to include are (1) the initial densities of the samples, (2) the quality of the experimental technique, and (3) whether the measurements were absolute or relative. All of the available data were taken using Al alloys with densities that differ from the known pure metal value of 2.70 g/cm^3 (predicted correctly by our EOS); some alloys are as close as 2.71 g/cm^3 while others differ much more. Since Hugoniots in general are quite sensitive to the initial density, we chose to compare only with the data for which ρ_0 clustered around 2.71 g/cm^3. (Thus we used only one data point from [20], which mainly concerns porous materials. All of the data from the other references were used.) We also avoided sources which gathered data using unusual shock wave geometries (such as [25]), and we also chose not to use the results of indirect or relative
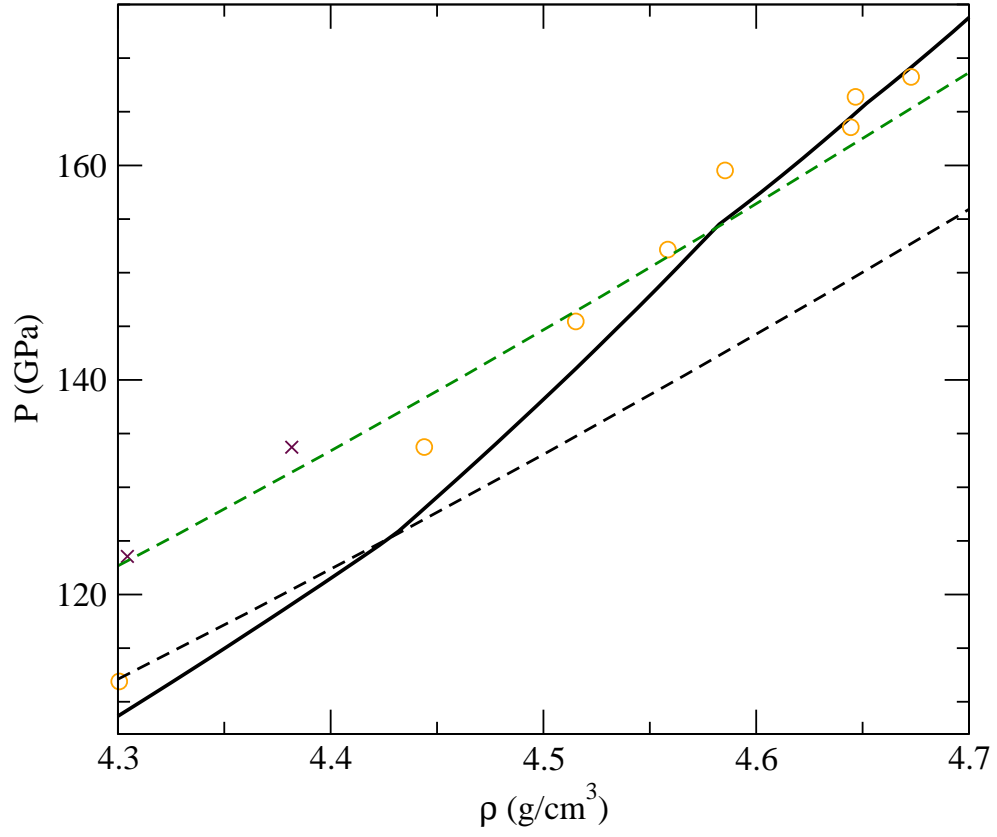
Figure 13: The P-ρ Hugoniot in the intermediate-P region, including intersections with the phase boundaries, with data from [23, 24].

measurements, such as [26, 27, 28], preferring to rely on the absolute measurements that are available. Finally, we did not use the few data points available (primarily nuclear-driven) that lie very far beyond the limits of applicability of our EOS (but see below).

The theoretical Hugoniot compares well with both the u_s-u_p and the P-ρ data all the way up to the predicted limit of its validity, at approximately 500 GPa (5 Mbar). More specifically, theory agrees with experiment at $P \stackrel{<}{\sim} 40$ GPa (Figures 10 and 11); at 40-125 GPa, theory falls below the experimental error bars by around 1% at most (Figures 10 through 13); and theory again lies within the experimental error bars through the liquid phase (Figures 8, 9, 12, and 13). (We recall that given percentage errors in u_s and u_p correspond to roughly the same percentage errors in the P-ρ plane.) The presence of theoretical error only in the solid phase is likely due to strength effects, which are present in the solid but not in the liquid, and which are neglected in our Hugoniot calculations. Furthermore, as Figure 13 shows, we predict that the Hugoniot crosses the two-phase region between $\rho = 4.43$ g/cm^3 and $\rho = 4.58$ g/cm^3, corresponding to a range in P from 126 to 156 GPa; this agrees very well with [14], in which melting was found to occur between 125 and 150 GPa. (We note that [14] used Al 2024, an alloy whose density is sufficiently different from pure Al that we did not use Hugoniot data taken with that alloy in our Figures. We consider their melting results because, as we saw in the previous Subsection, their data are consistent with other experiments that did use pure Al.) The correction to Φ_0^s from the previous Subsection, shown in Figure 3, shifts the Hugoniot at pressures below 30 GPa, bringing it into excellent agreement with experiment, while at pressures above 60 GPa or so, the effect on the Hugoniot is insignificant.

We have also compared our results with data just beyond the EOS limits of validity; the points in [29] that match our initial density (one of which is a reanalysis of the single point in [30]), lying at about 10 Mbar, fall noticeably below our Hugoniot, and their consistency with the very-high-pressure points of Ragan [31, 32] strongly suggests that they represent the true Hugoniot, which thus falls beneath our prediction at higher pressures. Possible errors in our EOS at such densities include, in what we estimate to be decreasing order of importance, (1) the shift from the fcc to the bcc crystal, with a corresponding change in Φ_0^l as discussed in the last Subsection, (2) deviations in the melt curve $T_m(P)$ from the Boehler-Ross form at higher pressures (the densities of the points in [29] correspond to melt pressures around 620 GPa according to our EOS), (3) the fact that at such high T the EOS is probing

the high-energy region of $n^s(\epsilon)$, and (4) the neglect of the anharmonic and boundary contributions to the liquid EOS (T is only slightly below $5\,T_m$ at these points according to our EOS).

4   Conclusions

Drawing upon theory developed in [2], we have described a framework for constructing EOS for elemental solids and liquids, and we have discussed experimental and theoretical results indicating that the framework remains highly accurate at low pressures when certain small effects (anharmonicity, boundaries, electron-phonon interactions) are neglected. After displaying the resulting formulas for the Helmholtz free energy, we considered the information one needs to evaluate them, and we discussed the combination of experiment and theoretical work that could be used to get this information. Finally, as an illustration we constructed an EOS for Al, established its range of validity based on the inputs to the EOS, and compared it with Hugoniot data to 5 Mbar; our EOS matched the data to the accuracy we expected based on the low-pressure results.

We consider the primary advantage of this method to lie in the fact that it incorporates into the decomposition of the Hamiltonian a great deal of accumulated knowledge of condensed matter physics both for the solid and liquid phases (for example, the fact that the electronic ground state energy is the most appropriate potential for the nuclear motion). If we have indeed captured the correct physics (and we expect no new physics to enter until the relativistic domain), then the EOS should have the right functional form, which means that if it is shown to agree with available data, then we have reason to believe that it will be equally accurate in regions where no data are available; and making predictions where we have no data is the point of having an EOS to begin with. Furthermore, the better the foundation we can build, the better our position for intelligently investigating and controlling our approximations.

This discussion bears on the second goal of this paper, which was to learn whether the approximation of neglecting anharmonic, boundary, and electron-phonon effects remains useful at higher pressures. We already knew, as discussed in the Introduction, that at low P the anharmonic and electron-phonon terms are small, and we found this from direct calculations; we also knew that for several elements, over a range of T, at low P the approxi-

31

mations in question yielded thermal energies and entropies that disagreed with experiments by 5% at most. Our work here has shown that for one material at much higher P the approximations yield results that match data along a single curve, the Hugoniot, to comparable accuracy. Based on our arguments above, that the EOS incorporates the correct physics and is thus of the correct functional form, we claim to have shown that this Al EOS is trustworthy throughout its range of validity, for all T and P.

The main disadvantage of this method is that it relies on many inputs (Φ_0, $g(\omega)$, and $n(\epsilon)$ for each phase) which may be available only over limited ranges, and each of these limits also restricts the range of validity of the EOS. Our Al example amply illustrates this problem; with a compression range from a little under one to just over two, and a temperature range that reaches only to slightly under 4 eV, this EOS is inadequate for many applications at the national laboratories. We argue, however, that this problem does not indicate a deficiency in the approach; it only underscores the need for many more DFT calculations of these quantities for more materials with ever greater accuracy over ever larger ranges.

In the meantime, though, we would like to be able to say something about elemental solid and liquid EOS at higher compressions. We do know that as density increases, the electrons come to dominate the free energy, and it is also known that TFD correctly describes the electrons in the limit of infinite density. This suggests the following possibility: Construct an EOS using the present techniques to compressions as high as the available experimental or DFT results allow, and then interpolate between these results and the predictions of TFD for higher compressions. This raises an important question: At what pressures does TFD begin to become accurate? Conventional wisdom, usually traced back to Feynman et al. [33], has held that TFD becomes reliable starting at $P \approx 10$ Mbar, but other work [34] suggests that TFD (or TF in their case, but TF and TFD converge at high pressures) deviates noticeably from electronic structure results until 100 Mbar at least. This suggests that the pressure threshold at which TFD is trustworthy has not yet been adequately established; it would be of great interest to settle this question more definitively.

Acknowledgment

References

[1] S. P. Lyon and J. D. Johnson, "T-1 Handbook of the Sesame Equation of State Library," Los Alamos Report LA-CP-98-100 (unpublished).

[2] D. C. Wallace, *Statistical Physics of Crystals and Liquids* (World Scientific, Singapore, 2003).

[3] M. Born and K. Huang, *Dynamical Theory of Crystal Lattices* (Oxford Univ Press, New York, 1988).

[4] E. D. Chisolm and D. C. Wallace, J. Phys.: Condens. Matter **13**, R739 (2001).

[5] D. C. Wallace and B. E. Clements, Phys. Rev. E **59**, 2942 (1999).

[6] E. D. Chisolm, B. E. Clements, and D. C. Wallace, Phys. Rev. E **63**, 031204 (2001); **64**, 019902 (2001).

[7] G. K. Straub, J. B. Aidun, J. M. Wills, C. R. Sanchez-Castro, and D. C. Wallace, Phys. Rev. B **50**, 5055 (1994).

[8] D. A. Young, *Phase Diagrams of the Elements* (Univ of California Press, Berkeley, 1991).

[9] H. Schober and P. H. Dederichs, in *Metals: Phonon States, Electron States and Fermi Surfaces*, edited by K.-H. Hellwege and J. L. Olsen, Landolt-Börnstein, New Series, Group III, Vol. 13, Pt. a (Springer-Verlag, Berlin, 1981).

[10] A. H. Wilson, *The Theory of Metals*, 2nd ed. (Cambridge Univ Press, Cambridge, 1954).

[11] J. McDougall and F. Stoner, Philos. Trans. R. Soc. London, Ser. A **237**, 67 (1938).

[12] P. Rhodes, Proc. Roy. Soc. London, Ser. A **204**, 396 (1950).

[13] R. Boehler and M. Ross, Earth Planet. Sci. Lett. **153**, 23 (1997).

[14] R. G. McQueen, J. N. Fritz, and C. E. Morris, in *Shock Waves in Condensed Matter 1983*, edited by J. R. Asay, R. A. Graham, and G. K. Straub (Elsevier Science Publishers, New York, 1984).

[15] A. Hänström and P. Lazor, J. Alloys Compd. **305**, 209 (2000).

[16] J. L. Pélissier, Physica **128A**, 363 (1984).

[17] J. A. Moriarty, D. A. Young, and M. Ross, Phys. Rev. B **30**, 578 (1984).

[18] N. W. Ashcroft and D. Stroud, in *Solid State Physics*, edited by F. Seitz, D. Turnbull, and H. Ehrenreich, Vol. 33, p. 1 (Academic, New York, 1978).

[19] L. V. Al'tshuler, S. B. Kormer, A. A. Bakanova, and R. F. Trunin, Sov. Phys. JETP **11**, 573 (1960).

[20] S. B. Kormer, A. I. Funtikov, V. D. Urlin, and A. N. Kolesnikova, Sov. Phys. JETP **15**, 477 (1962).

[21] *LASL Shock Hugoniot Data*, edited by S. P. Marsh (Univ of California Press, Berkeley, 1980).

[22] L. V. Al'tshuler, A. A. Bakanova, I. P. Dudoladov, E. A. Dynin, R. F. Trunin, and B. S. Chekin, J. Appl. Mech. Techn. Phys. **22**, 145 (1981).

[23] A. C. Mitchell and W. J. Nellis, J. Appl. Phys. **52**, 3363 (1981).

[24] M. D. Knudson, R. W. Lemke, C. A. Hall, C. Deeney and J. R. Asay, J. Appl. Phys. (in press).

[25] I. C. Skidmore and E. Morris, in *Thermodynamics of Nuclear Materials*, p. 173 (International Atomic Energy Association, Vienna, 1962).

[26] L. V. Al'tshuler, N. N. Kalitkin, L. V. Kuz'mina, and B. S. Chekin, Sov. Phys. JETP **45**, 167 (1977).

[27] R. F. Trunin, Bull. Acad. Sci. USSR, Phys. Ser. (Engl. Transl.) **22**, 103 (1986).

[28] B. L. Glushak, A. P. Zharkov, M. V. Zhernokletov, V. Ya. Ternovoi, A. S. Filimonov, and V. E. Fortov, Sov. Phys. JETP **69**, 739 (1989).

[29] V. A. Simonenko, N. P. Voloshin, A. S. Vladimirov, A. P. Nagibin, V. N. Nogin, V. A. Popov, V. A. Vasilenko, and Yu. A. Shoĭdin, Sov. Phys. JETP **61**, 869 (1985).

[30] A. P. Volkov, N. P. Voloshin, A. S. Vladimirov, V. N. Nogin, and V. A. Simonenko, JETP Lett. **31**, 588 (1980).

[31] C. E. Ragan, Phys. Rev. A **25**, 3360 (1982).

[32] C. E. Ragan, Phys. Rev. A **29**, 1391 (1984).

[33] R. P. Feynman, N. Metropolis, and E. Teller, Phys. Rev. **75**, 1561 (1949).

[34] W. G. Zittel, J. Meyer-ter-Vehn, J. C. Boettger, and S. B. Trickey, J. Phys. F: Met. Phys. **15**, L247 (1985).